doi: 10.29382/eqs-2019-0072-04

# Numerical modeling of global seismic phases and its application in seismic phase identification*

Chanjun Jiang[1,2] Youxue Wang[1,2,✉] Bin Xiong[1,2] Qianci Ren[1,2] Jinfeng Hu[1] Wenqi Gao[1] Yi Tian[1] Xi Zhuo[1]

[1] *School of Earth Science*, *Guilin University of Technology*, *Guilin* 541006, *China*
[2] *Guangxi Key Laboratory of Hidden Metallic Ore Deposits Exploration*, *Guilin* 541006, *China*

**Abstract** Earthquake data include informative seismic phases that require identification for imaging the Earth's structural interior. In order to identify the phases, we created a numerical method to calculate the traveltimes and raypaths by a shooting technique based upon the IASP91 Earth model, and it can calculate the traveltimes and raypaths for not only the seismic phases in the traditional traveltime tables such as IASP91, AK135, but also some phases such as pPcP, pPKIKP, and PPPPP. It is not necessary for this method to mesh the Earth model, and the results from the numerical modeling and its application show that the absolute differences between the calculated and theoretical traveltimes from the ISAP91 tables are less than 0.1 s. Thus, it is simple in manipulation and fast in computation, and can provide a reliable theoretical prediction for the identification of a seismic phase within the acquired earthquake data.

**Keywords**: IASP91 Earth model; numerical modeling; shooting method; seismic phase prediction

## 1 Introduction

Since the groundbreaking work of Aki and Lee (1976), who applied seismic tomography in their research of the velocity structure of the Earth's interior, earthquake data has become an important resource used to image the inner structure and heterogeneity of the Earth (Aki and Lee, 1976; Anderson and Dziewonski, 1982; Thomsen, 1986; Nolet, 1987; Chapman and Pratt, 1992; Engdahl et al., 1998; Rawlinson and Sambridge, 2003; Zhao and Lei, 2004; Zhang et al., 2011). The computation of the parameters of seismic waves, such as the travel times and ray paths from an event source to a detection station for global seismic phases, has become a key step. For this purpose, numerical modeling is an effective method for computing the parameters of a seismic wave based on previous Earth models (e.g., PREM model, Dziewonski and Anderson 1981; IASP91 model, Kennett and Engdahl 1991; AK135 model, Kennett et al., 1995).

For the numerical model to compute the travel times and ray paths of the seismic wave from an event source to a station that detects global seismic phases, raytracing always plays an important role. At the regional scale, there exists several 3-D raytracing algorithms for tomographic imaging (Steck et al., 1998; Bijwaard and Spakman,1999; Keyser et al., 2002; Zhao and Lei, 2004; Vidale and Helmberger, 1988, Vidale, 1990; K Kvasnička 1994; Rawlinson and Sambridge, Bai et al., 2010; Huang et al., 2013). Ho st global traveltime tomographic procedures simple ray tracing method through a one-dimensional (1-D) reference velocity model in the forward modelling process because there are usually millions of multiphase traveltime data entries that are involved. That is, ray paths are only calculated for a 1-D velocity model where velocity changes with depth or (radius) alone (e.g., the IASP91 model, Kennett and Engdahl, 1991, or the AK135 model, Kennett et al., 1995), and the ray nodes can be projected on the real location along the ray path from source to station during the inversion process. Most of the methods mentioned above used a grid/cell-based wavefront construction for the two-point solver.

Due to the enormous amount of earthquake data that can be acquired from a portable seismic array, phase identification is another key step in data processing. In order to determine the precise property of an unknown phase, theoretical traveltimes, such as those from the Jeffreys and Bullen tables (Jeffreys and Bullen, 1940), IASP91 tables (Kennett and Engdahl, 1991) and AK135 tables (Kennett, 2005; Snoke, 2009), are usually used to

* **Received** 17 March 2019; **accepted in revised form** 23 September 2019; **published** 26 March 2020.

✉ **Corresponding author. e-mail**: uxue.wang@glut.edu.cn

mark the onset time for global seismic phases by automatic or interactive methods, such as the STA/LTA method (Stevenson, 1976), AIC method (Sleeman and Van Eck, 1999), matched filter technique (Gibbons and Ringdal, 2006), FAST method (Brown et al., 2008), BP method (Rumelhart et al., 1988), and GEOTOOL (Coyne and Henson, 1995a,b) in the Unix/Linux environment, in order to determine accurate arrivals.

In this study, based on the IASP91 Earth model, we used a shooting method with a non-meshing scheme to trace ray paths and calculate the traveltimes of global seismic phases. We will use this method herein to process seismic data received from the broadband portable seismic array in Guangxi.

## 2 Ray tracing

In three-dimensional (3-D) media, the propagation of seismic waves satisfies the eikonal equation

$$(\nabla\tau)^2 = \frac{1}{v^2}, \tag{1}$$

where $\tau$ denotes the wavefront and $v$ denotes the velocity of the medium, and both are spatial functions of $(x, y, z)$.

Equation (1) in a Cartesian coordinate system can be rewritten as

$$\left(\frac{\partial\tau}{\partial x}\right)^2 + \left(\frac{\partial\tau}{\partial y}\right)^2 + \left(\frac{\partial\tau}{\partial z}\right)^2 = \frac{1}{v^2}. \tag{2}$$

In a 3-D case, three directional cosines at a point along the ray are introduced (Červeny et al., 1977), such as $\cos\theta_x = \frac{\partial x}{\partial s}$, $\cos\theta_y = \frac{\partial y}{\partial s}$, $\cos\theta_z = \frac{\partial z}{\partial s}$, where $\theta_x$, $\theta_y$, $\theta_z$ are the angles between the tangent and $x$, $y$ and $z$ axes at the point along the ray, respectively, and $s$ is the ray length. Thus, the kinematic equation for ray tracing can be written as

$$\begin{cases} \dfrac{\partial x}{\partial\tau} = v\cos\theta_x \\ \dfrac{\partial y}{\partial\tau} = v\cos\theta_y \\ \dfrac{\partial z}{\partial\tau} = v\cos\theta_z \\ \dfrac{\partial\theta_x}{\partial\tau} = \dfrac{\partial v}{\partial x}\sin\theta_x - \dfrac{\partial v}{\partial y}\cot\theta_x\cos\theta_y - \dfrac{\partial v}{\partial z}\cot\theta_x\cos\theta_z \\ \dfrac{\partial\theta_y}{\partial\tau} = \dfrac{\partial v}{\partial y}\sin\theta_y - \dfrac{\partial v}{\partial x}\cot\theta_x\cos\theta_y - \dfrac{\partial v}{\partial z}\cot\theta_y\cos\theta_z \\ \dfrac{\partial\theta_z}{\partial\tau} = \dfrac{\partial v}{\partial z}\sin\theta_z - \dfrac{\partial v}{\partial x}\cot\theta_x\cos\theta_z - \dfrac{\partial v}{\partial y}\cot\theta_x\cos\theta_y \end{cases}. \tag{3}$$

For the IASP91 Earth model, the velocity varies only with the radial radius, and therefore, the Earth model can be considered as a two-dimensional medium that is a section of a circle passing through the center of the core. In this situation, the velocity is only a function of 2D spatial coordinates, such as $x$ and $z$. If it is postulated that $\theta_x = \alpha$, $\theta_y = \frac{\pi}{2}$, $\theta_z = \frac{\pi}{2} - \alpha$ (Červeny et al., 1977) Equation (3) can be simplified as

$$\begin{cases} \dfrac{\partial x}{\partial\tau} = v\cos\alpha \\ \dfrac{\partial z}{\partial\tau} = v\sin\alpha \\ \dfrac{\partial\alpha}{\partial\tau} = \dfrac{\partial v}{\partial x}\sin\alpha - \dfrac{\partial v}{\partial z}\cos\alpha \end{cases}. \tag{4}$$

After it is discretized, Equation (4) becomes

$$\begin{cases} x = x_0 + v\cos\alpha_0 \cdot \Delta\tau \\ z = z_0 + v\sin\alpha_0 \cdot \Delta\tau \\ \alpha = \alpha_0 - (v_x\sin\alpha_0 - v_z\cos\alpha_0)\cdot\Delta\tau \end{cases}, \tag{5}$$

where $(x_0, z_0)$ are the coordinates of the ray starting point $S$, $(x, z)$ are the coordinates of the point $P$ along the ray (Figure 1), $\alpha_0$ and $\alpha$ are the take-off angles at points $S$ and $P$, respectively, and $\Delta\tau$ is the time step during the ray tracing.

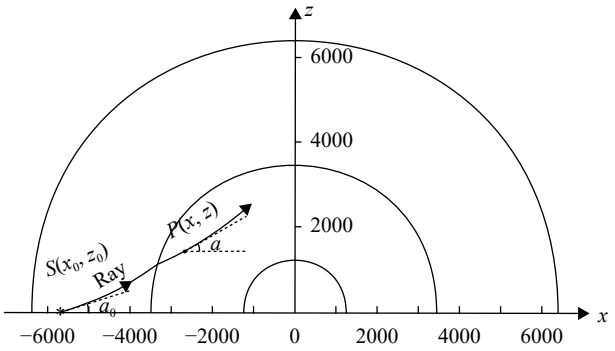


**Figure 1** Diagram for ray tracing

During the process of ray tracing, a global seismic phase, such as P, PcP, SKIKP, or PKiKS, was coded into a series of ray codes code($k$), $k$=1,2, … first (i.e., for PcS, code(1)=P, code(2)=c, code(3)=S). Then, the initial take-off angle will be interpolated by the empirical ranges of the take-off angle for different phases with different focus depths.

This method does not need to mesh the reference model, and the ray is traced layer by layer using a shooting method for a pair of source stations. For a specific phase or ray code, the initial take-off angle $\alpha_0$ will be interpolated with the focus depth by the empirical ranges of take-off angles. The ray starts at source $(x_0, z_0, \alpha_0)$ where the velocity is $v_0$, and the ray will propagate within the layer in which the ray is currently located by a time step $\Delta\tau$ using Equation (5) to generate the next ray point $(x, z, \alpha)$, where

the velocity is $v$. Then, ($x_0$, $z_0$, $\alpha_0$) is replaced by ($x$, $z$, $\alpha$) iteratively until the ray arrives at the boundary (upper or lower) of the layer. The velocity at any ray point can be calculated by the velocity-depth (radius) function provided by the IASP91 Earth model. When finishing the tracing in the layer and before the ray enters the next layer, it is necessary for the parameter $\alpha$ to be recalculated by Snell's law for reflection or refraction according to the ray code. When the ray arrives at the surface, if the ray does not arrive at the station, the initial take-off angle requires adjustment for another round of tracing until the ray arrives at the station.

The ray with a different phase penetrates at a different depth, and the empirical ranges of the take-off angle will provide a limitation for the propagation of the ray. For example, the ray for the P phase does not touch the mantle/core boundary and propagates above the boundary. For a reflection such as PcP, in addition to the range limitation of the take-off angle, another constraint is that the ray must hit the mantle/core boundary, and the ray must be reflected at the hit-point on the boundary.

The time step $\tau$ should be assigned a reasonable value to ensure the accuracy of the tracing. Through several tests in this study, it was determined that the value $\tau$=0.01 s can satisfy the accuracy of the traveltimes from the IASP91 traveltime tables.

## 3 Numerical modeling of seismic phases

Based upon the IASP91 Earth model (Kennett and Engdahl, 1991), the different seismic phases traveling through the Earth are modeled by a ray tracing technique, including traveltimes and ray trajectories. The IASP91 Earth model and seismic phases are shown in Table 1 and Figure 2.

To evaluate the reliability of the ray tracing used in this study, the phases used by Knettett and Engdahl (1991) were calculated with a focal depth of 0.0 km and a time

**Table 1** The parameters of IASP91 Earth model

| Radius (km) | $v_P$ (km/s) | $v_S$ (km/s) |
|---|---|---|
| 6351–6371 | 5.8 | 3.36 |
| 6336–6351 | 6.5 | 3.75 |
| 6251–6336 | 8.78541–0.749530$x$ | 6.706231–2.248585$x$ |
| 6161–6251 | 25.41389–17.69722$x$ | 5.750200–1.274200$x$ |
| 5961–6161 | 30.78765–23.25415$x$ | 15.242130–11.085520$x$ |
| 5711–5961 | 29.38896–21.40656$x$ | 17.707320–13.506520$x$ |
| 5611–5711 | 25.96984–16.93412$x$ | 20.768900–16.531470$x$ |
| 3631–5611 | 25.14860–41.15380$x$+51.99320$x^2$–26.60830$x^3$ | 12.930300–21.259000$x$+27.89880 $x^2$–14.10800 $x^3$ |
| 3482–3631 | 14.49470–1.47089$x$ | 8.166160–1.582060$x$ |
| 1217–3482 | 10.03904+3.75665$x$–13.67046$x^2$ | 0 |
| 0–1217 | 11.24094–4.09689$x^2$ | 3.564540–3.452410$x^2$ |

Note: $x$=$r$/$R$, where $r$ is the radius from the Earth center, $R$ is the Earth's radius ($R$=6371.00 km)

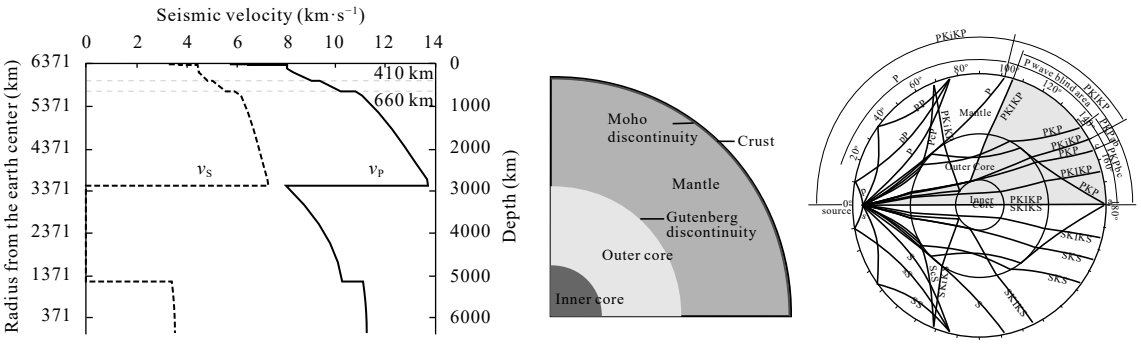


**Figure 2** IASP91 Earth model and seismic phases

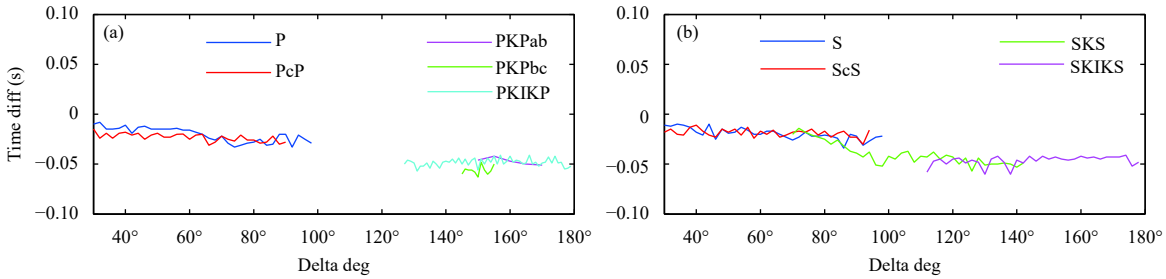


**Figure 3** Time differences between the calculated and theoretical traveltimes

step of 0.01 s, and it was determined that the differences between the calculated and theoretical traveltimes were less than 0.1 s (Figure 3). In addition to the phases calculated above, the other phases, such as PP, PS, SS, PSP, ScP, PKS, PKIKS, PkiKP, and SKiKS, were also computed (Figures 4 and 5). The CPU times for calculating phase P and PKIKP are given in Table 2.

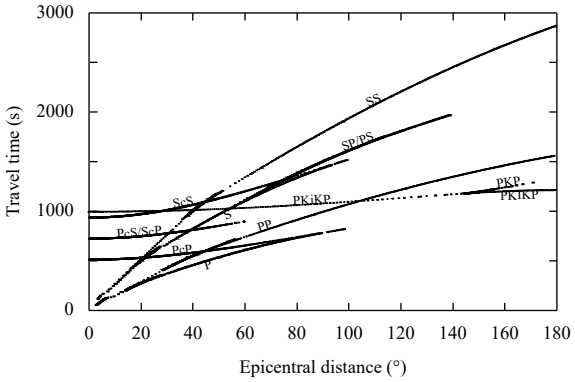


**Figure 4** Time-distance curves for different seismic phases

**Table 2** CPU times for caculating phases

| Seismic phase | Delta deg (interval=2°) | CPU time (s) |
|---|---|---|
| P | 30°–90° | 44.652 |
| PKIKP | 140°–176° | 10.130 |

Note: The CPU time includes tracing and plotting

## 4 Application in seismic phase identification

A portable seismic array was deployed in Guangxi during 2014–2018. In order to obtain more accurate traveltime in this region to mark the onset time, the IASP91 model was modified by the crustal structure (Huang, 2000). The data used were a 20-km upper crust with a velocity of 6.2 km/s and a 10-km lower crust with a velocity of 6.9 km/s, and a total thickness of the crust of approximately 30 km. The earthquake events were acquired from a portable seismic array in Guangxi, and it was necessary for the seismic phases to be identified and confirmed by numerical modeling before they could be used to image the Earth's structure, including wave arrivals and their attributes. In this study, the earthquake data from the portable seismic array in Guangxi were used for numerical modeling (Tables 3 and 4, Figure 6), and the results are given in Figure 7.

It can be seen from Figure 7 that the synthetic traveltime of the predicted phases based on the IASP91 Earth model are consistent with the arrivals recorded by the Guangxi portable seismic array, which received the seismic data from the Nepal event (#1), with a distance approximately 23.8 degrees, and the Chile event (#2), with a distance of approximately 160.0 degrees. In these two events, in addition to the main phases that were determined, such as P, S, PKIKP, and Rayleigh waves, some multiple reflection phases of PP, SS, PPP, PPPP, PPPPP and converted phase PS were also determined. There are certain time differences that existed between the predicted and actual arrivals that provide a possibility for studying the Earth's structure interior, including radial and lateral inhomogeneities of the Earth.

## 5 Conclusions

Based upon the IASP91 Earth model and adapting the ray tracing technique, numerical modeling was carried out to calculate the traveltimes and raypaths of different seismic phases that propagate through the Earth's interior. The results from the numerical modeling and its application show that

1) this method can reveal the kinematic characteristics of seismic phases propagating through the Earth's interior;

2) this method does not need to mesh the Earth model, and therefore, it is simple in manipulation and fast in computation with a high accuracy, and the differences between the calculated and theoretical traveltime are less than 0.1 s;

3) according to the local crust structure, the method permits the user to modify the IASP91 model to obtain more accurate traveltimes to mark the onset time for

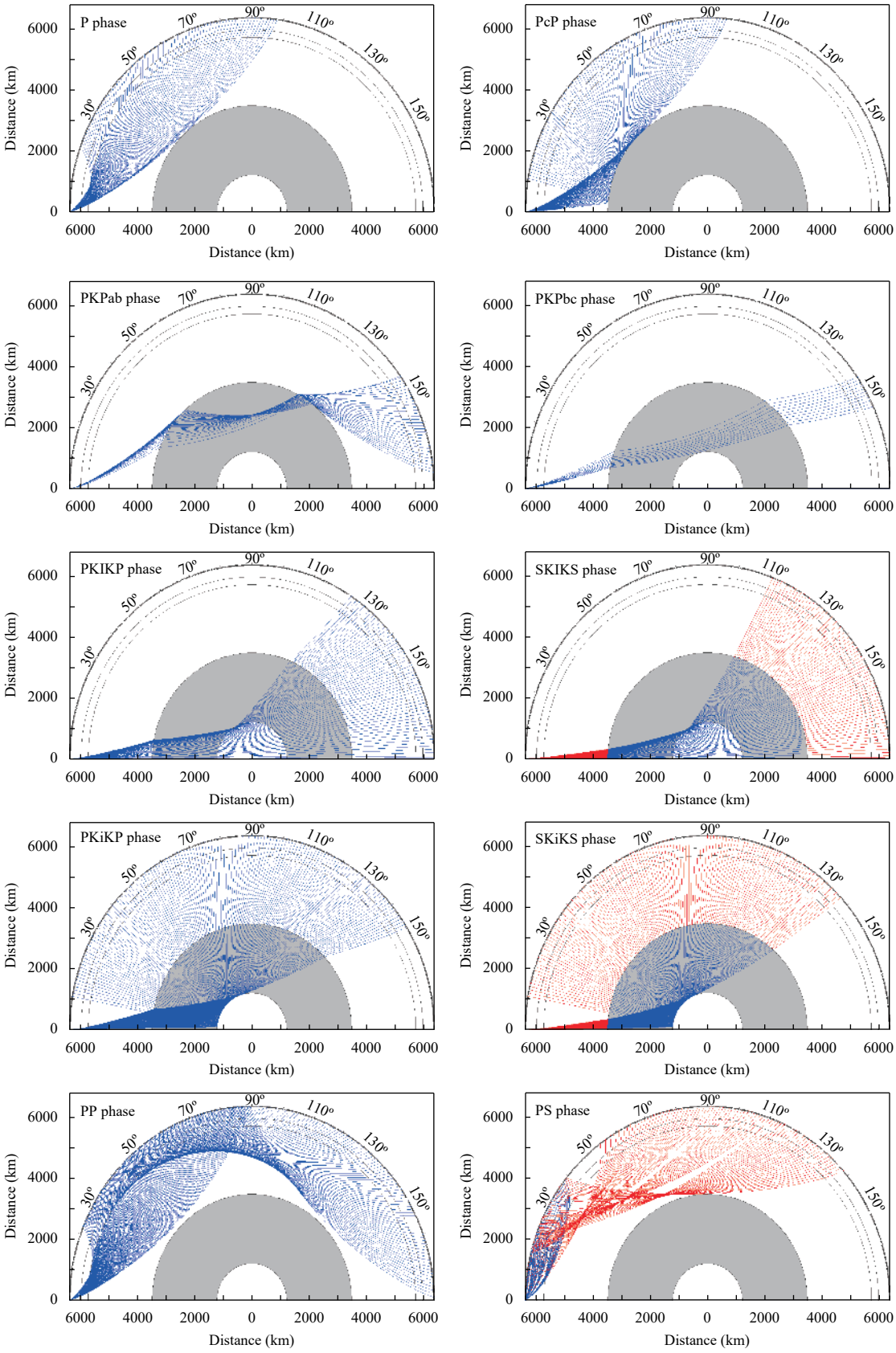


**Figure 5** The raypaths for different seismic phases. The source depth is 0 km; blue lines denote P-waves, and red lines denote S-waves

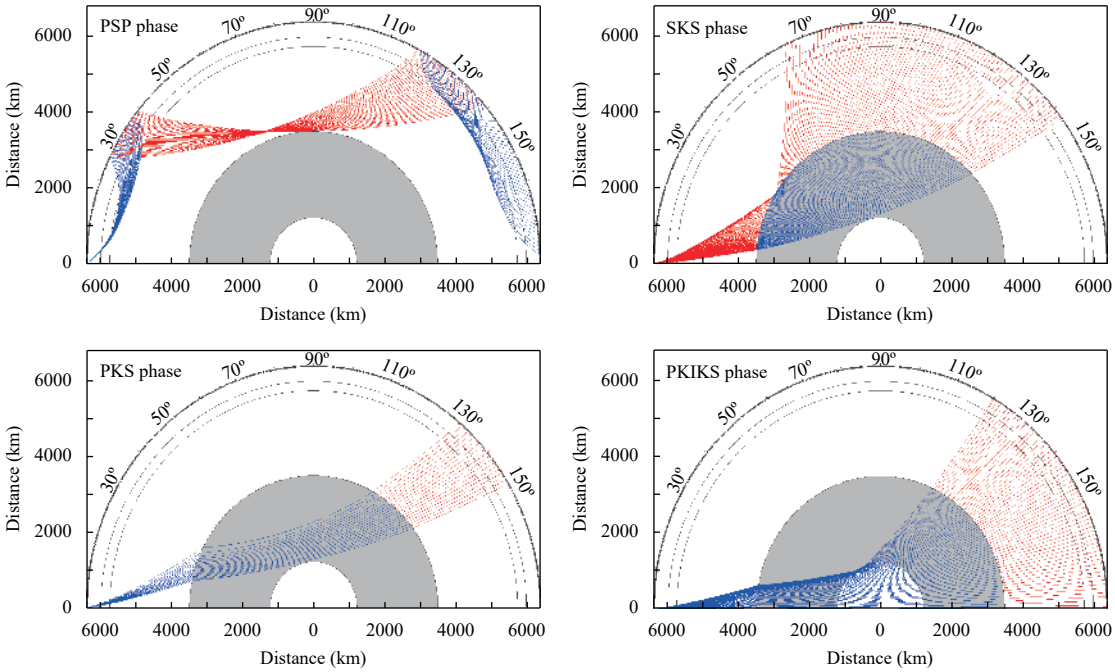


**Figure 5** Continued

**Table 3** Parameters of events

| No. of event | Event date a-mo-d | Origin time (UTC) h:min:s | Latitude (°N) | Longitude (°E) | Source depth (km) | Magnitude |
|---|---|---|---|---|---|---|
| #1 | 2015-04-25 | 06:11:26.27 | 28.1473 | 84.7079 | 15.00 | 7.80 |
| #2 | 2016-12-25 | 14:22:27.05 | –43.4029 | –73.9395 | 38.00 | 7.60 |

**Table 4** Parameters for the seismic stations

| Event #1 (Nepal) | | | | Event #2 (Chile) | | | |
|---|---|---|---|---|---|---|---|
| Station name | Latitude (°N) | Longitude (°E) | Altitude (m) | Station name | Latitude (°N) | Longitude (°E) | Altitude (m) |
| XX11 | 22.49661 | 111.99059 | 66.0 | NY21 | 26.03264 | 112.02917 | 594.0 |
| YA11 | 23.01133 | 111.99178 | 39.0 | HD21 | 23.99810 | 108.52300 | 136.0 |
| HJ11 | 23.50741 | 111.99253 | 289.0 | NN21 | 23.01030 | 108.47080 | 164.0 |
| YN11 | 23.00456 | 111.48505 | 113.0 | JY21 | 25.02711 | 111.02261 | 339.0 |
| FK11 | 23.49851 | 111.49821 | 55.0 | JX21 | 24.00762 | 109.98574 | 183.0 |
| WZ11 | 23.00001 | 111.01124 | 133.0 | BB21 | 24.50182 | 111.49850 | 153.0 |
| CW11 | 23.49256 | 110.98616 | 35.0 | ZP21 | 24.00410 | 111.02145 | 120.0 |
| WY11 | 23.00802 | 110.49465 | 144.0 | GP21 | 23.99706 | 111.99180 | 66.0 |
| QT11 | 22.99568 | 109.51865 | 51.0 | FK11 | 23.49851 | 111.49821 | 55.0 |
| SB11 | 23.50738 | 109.49126 | 135.0 | PP11 | 22.50009 | 110.49078 | 153.0 |
| ZC11 | 23.01179 | 109.00520 | 86.0 | FS21 | 22.00110 | 109.99447 | 84.0 |
| | | | | YD21 | 22.03144 | 111.98484 | 42.0 |

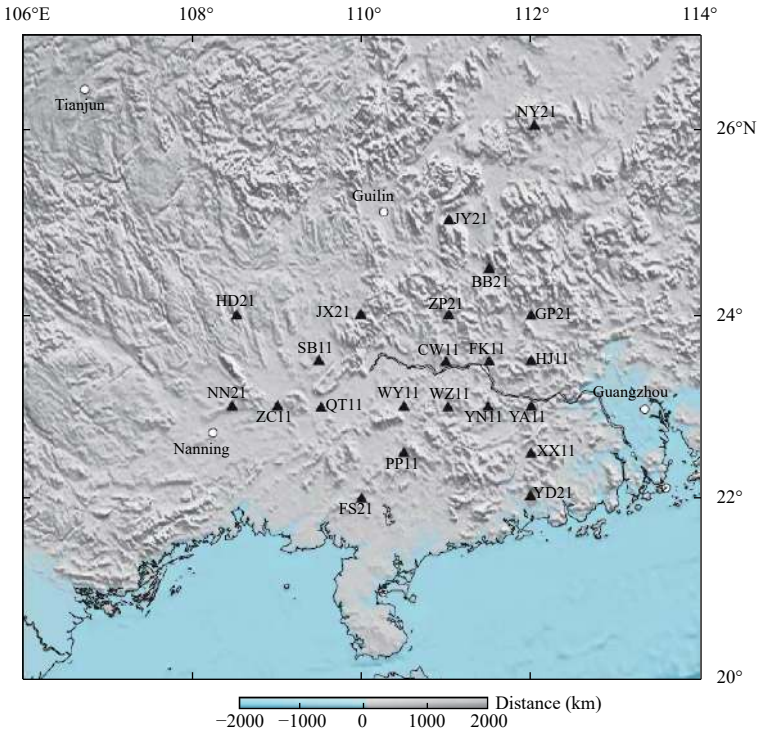


**Figure 6** Location map of the portable seismic stations in Guangxi, China

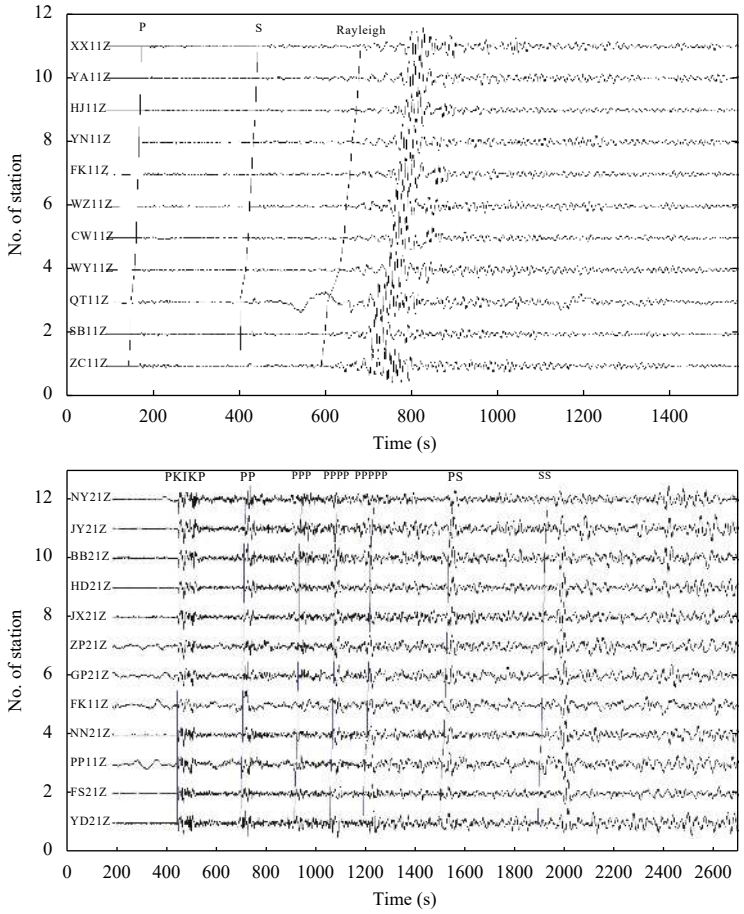


**Figure 7** The seismic phases and modeled results for event #1 (top) and event #2 (below)

different global seismic phases;

4) with the graphical user interface (GUI) in the Microsoft Windows environment, it is friendly and flexible and allows users to easily calculate a specified phase, such as some phases that cannot be found in existing traveltime tables.

## References


Aki K and Lee WHK (1976) Determination of three-dimensional velocity anomalies under a seismic array using first P arrival times from local earthquakes: 1. A homogeneous initial model. J Geophys Res **81**(23): 4 381–4 399

Anderson DL and Dziewonski AM (1982) Upper mantle anisotropy: Evidence from free oscillations. Geophys J Int **69**(2): 383–404

Bai CY, Huang GJ and Zhao R (2010) 2-D/3-D irregular shortest-path ray tracing for multiple arrivals and its applications. Geophys J Int **183**(3): 1 596–1 612

Bijwaard H and Spakman W (1999) Fast kinematic ray tracing of first-and later-arriving global seismic phases. Geophys J Int **139**(2): 359–369

Brown JR, Beroza GC and Shelly DR (2008) An autocorrelation method to detect low frequency earthquakes within tremor Geophys Res Lett **35**(16): L16 305

Červený V, Molotkov IA, Molotkov IA and Pšenčík I (1977) Ray Method in Seismology. Praha, Univerzita Karlova, pp33–35.

Chapman CT and Pratt RG (1992) Traveltime tomography in anisotropic media—I. Theory. Geophysical Journal International **109**(1): 1–19

Coyne JM and Henson I (1995a) *Geotool Sourcebook: User's Manual*. TELEDYNE BROWN ENGINEERING HUNTSVILLE AL.

Coyne JM and Henson I (1995b) *Further Development of the Geotool Seismic Analysis System* (No. C95-01). TELEDYNE BROWN ENGINEERING HUNTSVILLE AL.

Dziewonski AM and Anderson DL (1981) Preliminary reference Earth model. Phys Earth Planet Interi **25**(4): 297–356

Engdahl ER, Van der Hilst RD and Buland R (1998) Global teleseismic earthquake relocation with improved travel times and procedures for depth determination. Bull Seismol Soc Am **88**: 722–743

Gibbons SJ and Ringdal F (2006) The detection of low magnitude seismic events using array-based waveform correlation. Geophys J Int **165**(1): 149–166

Huang GJ, Bai CY and Greenhalgh S (2013) Fast and accurate global multiphase arrival tracking: The irregular shortest-path method in a 3-D spherical Earth model. Geophys J Int **194**(3): 1 878–1 892

Jeffreys H and Bullen KE (1940) Seismological tables. British Association for the Advancement of Science, London.

Kennett BLN and Engdahl ER (1991) Travel times for global earthquake location and phase association Geophys J Int **105**: 429–465

Kennett BLN, Engdahl ER and Buland R (1995) Constraints on seismic velocities in the Earth from traveltimes. GeophysJ Int **122**: 108–124

Kennett BLN (2005) Seismological Tables: AK135. Research School of Earth Sciences Australian National University Canberra, Australia pp1–289

Keyser M, Ritter JR and Jordan M (2002) 3D shear-wave velocity structure of the Eifel plume, Germany. Earth Planet Sci Lett **203**(1): 59–82

and Kvasnička M (1994) 3-D network ray tracing. ys J Int **116**(3): 726–738

987) Seismic wave propagation and seismic tomography. *mic Tomography*. Springer, Dordrecht, pp 1–23

Rawlinson N and Sambridge M (2004a) Wave front evolution in strongly heterogeneous layered media using the fast marching method. Geophys J Int **156**(3): 631–647

Rawlinson N and Sambridge M (2003) Seismic traveltime tomography of the crust and lithosphere. Advances in Geophysics **46**: 81–199

Rawlinson N and Sambridge M (2004b) Multiple reflection and transmission phases in complex layered media using a multistage fast marching method. Geophysics **69**(5): 1 338–1 350

Rumelhart DE, Hinton GE and Williams RJ (1988) Learning representations by back-propagating errors. Cognitive Modeling **5**(3): 1

Sleeman R and Van Eck T (1999) Robust automatic P-phase picking: An on-line implementation in the analysis of broadband seismogram recordings. Phys Earth Planet Interi **113**(1-4): 265–275

Snoke JA (2009) Traveltime tables for Iasp91 and Ak135. Seismol Res Lett **80**(2): 260–262

Stevenson PR (1976) Microearthquakes at Flathead Lake, Montana: A study using automatic earthquake processing. Bull Seismol Soc Am **66**(1): 61–80

Steck LK, Thurber CH, Fehler MC, Lutter WJ, Roberts PM, Baldridge WS and Sessions R (1998) Crust and upper mantle P wave velocity structure beneath Valles caldera, New Mexico: Results from the Jemez teleseismic tomography experiment. J Geophys Res : Solid Earth **103**(B10): 24 301–24 320

Thomsen L (1986) Weak elastic anisotropy. Geophysics **51**(10): 1 954–1 966

Vidale JE and Helmberger DV (1988) Elastic finite-difference modeling of the 1971 San Fernando, California earthquake. Bull Seismol Soc Am **78**(1): 122–141

Vidale JE (1990) Finite-difference calculation of traveltimes in three dimensions. Geophysics **55**(5): 521–526

Zhao D and Lei J (2004) Seismic ray path variations in a 3D global velocity model. Phys Earth Planet Interi **141**(3): 153–166

Zhang FX, L i YH, Wu QJ and Ding ZF (2011) The P phase veloctiy structure of upper mantle beneath the North China and surrounding regions from FMTT. Chin J Geophys **54**(5): 1 233–1 242